Published in final edited form as:
J Magn Reson Imaging. 2012 October ; 36(4): 890–899. doi:10.1002/jmri.23713.

High Resolution Navigated 3D T_1-weighted Hepatobiliary MRI using Gadoxetic Acid Optimized for 1.5T

Scott K. Nagle, MD, PhD[1,2], **Reed F. Busse, PhD**[3], **Anja C. Brau, PhD**[4], **Jean H. Brittain, PhD**[3], **Alex Frydrychowicz, MD**[5], **Yuji Iwadate, MS**[6], and **Scott B. Reeder, MD, PhD**[1,2,7,8]

[1]Department of Radiology, University of Wisconsin, Madison, WI

[2]Department of Medical Physics, University of Wisconsin, Madison, WI

[3]Global Applied Science Lab, GE Healthcare, Madison, WI

[4]Global Applied Science Lab, GE Healthcare, Menlo Park, CA

[5]Department of Radiology, University of Lübeck, Lübeck, Germany

[6]Global Applied Science Lab, GE Healthcare Japan, Hino, Japan

[7]Department of Biomedical Engineering, University of Wisconsin, Madison, WI

[8]Department of Medicine, University of Wisconsin, Madison, WI

Abstract

Purpose—To determine optimal delay times and flip angles for T1-weighted hepatobiliary imaging at 1.5T with gadoxetic acid and to demonstrate the feasibility of using a high-resolution navigated optimized T1-weighted pulse sequence to evaluate biliary disease.

Materials and Methods—Eight healthy volunteers were scanned at 1.5T using a T1-weighted 3D-SPGR pulse sequence following the administration of 0.05 mmol/kg of gadoxetic acid. Navigator-gating enabled acquisition of high spatial resolution ($1.2 \times 1.4 \times 1.8$ mm^3, interpolated to $0.7 \times 0.7 \times 0.9$ mm^3) images in approximately 5 minutes of free breathing. Multiple breath-held acquisitions were performed at flip angles between 15° and 45° to optimize T1 weighting. To evaluate the performance of this optimized sequence in the setting of biliary disease, the image quality and biliary excretion of 51 consecutive clinical scans performed to assess primary sclerosing cholangitis (PSC) were evaluated.

Results—Optimal hepatobiliary imaging occurs at 15–25 minutes, using a 40° flip angle. The image quality and visualization of biliary excretion in the PSC scans were excellent, despite the decreased liver function in some patients. Visualization of reduced excretion often provided diagnostic information that was unavailable by conventional magnetic resonance cholangiopancreatography (MRCP).

Conclusion—High-resolution navigated 3D-SPGR hepatobiliary imaging using gadoxetic acid and optimized scan parameters is technically feasible and can be clinically useful, even in patients with decreased hepatobiliary function.

Keywords

magnetic resonance; liver imaging; navigator; gadoxetic acid; optimization; primary sclerosing cholangitis

Correspondence: Scott K. Nagle, MD, PhD, Department of Radiology, University of Wisconsin, 600 Highland Avenue, Madison, WI 53792-3252, phone 608-265-6429, fax 608-262-6214, snagle@uwhealth.org.

INTRODUCTION

Since the development of rapid 3D breath-hold T1-weighted fat-saturated pulse sequences for volumetric imaging of the liver in the late 1990's (1), the use of gadolinium-based contrast agents (GBCA) for dynamic contrast imaging of the liver has become firmly established for the evaluation of hepatobiliary disease. In addition, two commercially available GBCAs – gadobenate dimeglumine (Multihance; Bracco Diagnostics, Princeton, NJ) and gadoxetic acid (Eovist; Bayer Pharmaceuticals, Wayne, NJ) – have been used as hepatobiliary contrast agents in conjunction with delayed T1 weighted imaging. Approximately 3–5% of gadobenate dimeglumine (2) and 50% of gadoxetic acid (3) are taken up by hepatocytes and subsequently excreted into the bile. Both agents have demonstrated a benefit for improved detection of metastases (4,5) as well as differentiation of hypervascular lesions such as focal nodular hyperplasia from hepatic adenoma (6,7). Exciting recent work also suggests improved diagnostic accuracy for detection and characterization of hepatocellular carcinoma (HCC) using these agents (8,9). In addition, the direct excretion of these agents into bile offers new possibilities for functional biliary imaging such as diagnosis of bile leaks, biliary obstruction and cholecystitis (10), in a manner similar to a nuclear scintigraphic hepatobiliary iminodiacetic acid (HIDA) scan, but with the high spatial resolution of MRI and the absence of ionizing radiation. The potential ability of T1-weighted 3D-SPGR imaging to detect and characterize focal abnormalities in biliary *function* may add important complementary information to conventional T2-weighted magnetic resonance cholangiopancreatography (MRCP) evaluation of biliary *structure* (11,12).

Rapid data acquisition methods with fat-saturated T1 weighted 3D spoiled gradient echo (3D-SPGR) are commonly used for dynamic contrast-enhanced imaging to capture arterial and portal venous phases during a single breath-hold. Parallel imaging can be used to improve spatial resolution through increased matrix sizes and an increased number of thinner slices (13). Ultimately, however, the maximum achievable spatial resolution obtainable during a breath-hold is limited by the signal-to-noise ratio (SNR), which decreases rapidly as voxel size decreases and higher parallel imaging acceleration factors are used.

Despite the widespread availability of these agents, there has been a relative paucity of imaging literature regarding optimization strategies that maximize the relative contrast between relevant tissues (*e.g.* liver and bile ducts) and the spatial resolution (14,15). Further, most reports of delayed 'hepatobiliary phase' imaging using these agents simply repeat the acquisition performed during dynamic phase imaging, without optimization that could improve SNR and CNR performance. During the dynamic arterial and portal venous phases, flip angles of approximately 15° are typically used to provide moderate T1-weighting with good SNR performance. However, concentrations of gadolinium in the liver tissue and bile may be dramatically different in the hepatobiliary phase as compared to the arterial and portal venous phases, and the optimal flip angle should therefore be re-examined.

During the hepatobiliary phase, contrast uptake and excretion into the bile are relatively slow and, for the purposes of delayed imaging, are in a pseudo-steady-state. For this reason, acquisition of delayed phase images does not require breath-holding and can be performed over a longer period of time (minutes). In this way, longer scan times can be translated into higher spatial resolution while maintaining adequate SNR performance. To acquire images during longer scans without artifacts from respiratory motion, however, strategies such as respiratory triggering or navigator pulses are necessary, as summarized recently by Asbach, *et. al.*(15).

The purpose of this work was three-fold: 1) to evaluate the ability of a navigator-based fat-saturated T1-weighted 3D-SPGR imaging method to obtain high spatial resolution hepatobiliary phase imaging in approximately 5 minutes of free-breathing, 2) to optimize key imaging parameters (delay following contrast administration and flip angle to optimize T1 weighting) for visualization of hepatic lesions and biliary anatomy when using gadoxetic acid, and 3) to demonstrate the feasibility of using this optimized navigated sequence in a patient population with expected abnormalities in biliary excretion.

MATERIALS AND METHODS

This HIPAA-compliant study received local Institutional Review Board approval. Eight (8) healthy subjects without liver disease (4:4 male:female), aged 40 ± 14 years (22–58 years) and weighing 82.5 ± 13.1 kg (63.5–104.3 kg), were recruited from an IRB-approved database of healthy volunteers. Each volunteer was scanned during a single study visit to determine optimal timing and flip angle for hepatobiliary phase imaging and to compare the image quality of the high-resolution navigated 3D-SPGR acquisition with a conventional breath-held 3D-SPGR sequence. All scans were performed on a 1.5T clinical scanner (Signa HDx, v14.0, GE Healthcare, Waukesha, WI), using an 8-channel phased array cardiac coil and an axial excitation centered on the upper abdomen of each subject in supine position. Using a 20G antecubital intravenous catheter, 0.05 mmol/kg of gadoxetic acid (Bayer Healthcare, Wayne, NJ) was injected using a power injector (Spectris Solaris, MedRad Inc., Warendale, PA) at 2 mL/s, followed by 20mL of saline flush at the same rate.

Navigated 3D-SPGR

An investigational version of a navigator-gated 3D-SPGR sequence was created by adding a periodic cylindrical excitation navigator pulse to the standard fat-saturated T1w 3D-SPGR sequence. The navigator consisted of a 25 ms cylindrical “pencil-beam” 2D RF excitation pulse, with long axis oriented perpendicular to the dome of the subject's right hemi-diaphragm. The width of the excitation was 10–20 mm and the length was 70–100 mm. A low 10° flip angle was used to avoid possible saturation in the imaging volume. The navigator echo was acquired at the end of each 200 ms imaging block, consisting of spectrally-selective partial fat inversion and segmented data acquisition. Translation of the diaphragm along the long axis of the navigator volume was calculated from the navigator echo in real time using an edge detection algorithm. Data from a particular imaging block were accepted only when the navigator-determined position of the diaphragm fell within the acceptance window positioned during end-expiration (±2 mm default width, manually adjustable during the scan); otherwise, data were rejected. For the purposes of this work, we will refer to this pulse sequence as “navigated 3D-SPGR”.

Optimal Delay Time

Each of the eight (8) healthy subjects was scanned for approximately 30 minutes following the contrast injection both to measure the pharmacokinetics of hepatobiliary enhancement and then to compare image quality between conventional breath-held and navigated 3D-SPGR methods. Image acquisition alternated between a breath-held 3D-SPGR acquisition without navigator pulses and a navigated 3D-SPGR acquisition, resulting in 46 pair-wise comparisons between the acquisition methods across all 8 subjects. Specific scan parameters are shown in Table 1. A flip angle of 15° was used for these scans, based upon the then-current routine clinical protocols for post-contrast T1-weighted SPGR of the abdomen at our institution. Parallel imaging acceleration was not used in order to maximize SNR performance and to allow accurate measurement of SNR ratios from the resulting images. The navigated 3D-SPGR scan time was variable, depending on each subject’s respiratory pattern. The navigated 3D-SPGR scans, which had higher spatial resolution than the breath-

hold acquisitions, were used for the timing analysis in order to improve the measurement of bile duct signal by decreasing the effect of volume averaging in these small structures.

Optimal Flip Angle

Beginning at approximately 30 minutes after contrast administration, multiple breath-held acquisitions were performed with flip angles varying from 15° to 45° (increments of 5°) in order to determine the optimal flip angles for hepatobiliary imaging that maximize the contrast between liver and both bile ducts and muscle. End-expiration breath-held 3D-SPGR imaging, rather than navigated 3D-SPGR, was used to acquire images at multiple different flip angles within a short period of time during which the amount of gadolinium in the liver, muscle, and bile ducts was assumed to remain constant. To ensure that any signal differences were due to flip angle rather than changes in gadolinium concentration, the flip angle order was reversed in 2 of the volunteers. Further, in 2 other volunteers, the 25° flip angle acquisition was repeated following all other acquisitions (approximately 10 minutes later) to demonstrate that tissue gadolinium concentrations remained effectively constant throughout the duration of the flip angle optimization.

Clinical Implementation

The optimized, navigated 3D-SPGR acquisition (using a flip angle of 40°) was implemented in clinical MRCP protocols as a biliary-phase acquisition beginning at 20 minutes following contrast injection. A HIPAA-compliant, IRB-approved retrospective review of fifty-one (51) consecutive clinical studies in 31 patients with known or suspected primary sclerosing cholangitis (PSC) was then performed. PSC is a condition with variable severity of biliary disease among patients, as well as variable biliary function, making it well-suited to test the feasibility of this optimized navigated 3D-SPGR acquisition. Patient demographics included: 21:10 male:female, ages: 47 ± 16 years (18–83 years), and weight: 81.6 ± 14.5 kg (50.3–113.0 kg). The overall image quality and visualization of biliary excretion was assessed.

To illustrate the potential additional utility of using the optimized, navigated 3D-SPGR in other diseases affecting biliary secretion, two additional clinical examples (non-hepatocyte origin intrahepatic neoplasm and suspected gallstone pancreatitis) are also shown and discussed.

Data Analysis

Qualitative Comparison of Breath-held and Navigated 3D-SPGR—The navigated 3D-SPGR images were compared with the conventional breath-held images by 2 radiologists with subspecialty training in MRI, using a consensus methodology. All scans (breath-held and navigated) were scored for image quality on a 4-point Likert scale (0=non-diagnostic, 1=severe artifact, 2=very mild artifact, and 3=no significant artifact). Breath-held and navigated 3D-SPGR image sets acquired at contiguous time points were then paired, and the raters were asked to choose which of the scans they preferred (1=breath-held preferred, 2=equivalent, 3=navigated preferred).

Optimization of Delay Time and Flip Angle—Data analysis was performed on magnitude images, using a clinical PACS workstation (McKesson, San Francisco, CA). A board-certified radiologist with fellowship training in abdominal MRI and 6 years of experience in diagnostic imaging drew regions of interest (ROI) in the liver, bile ducts, muscle, and air (4 ROIs, one in each corner of the image) at the same anatomic location and with the same size on all of the comparison scans of each subject. Muscle 9 signal, which is commonly used as a surrogate for neoplastic lesions of non-hepatocyte origin (*e.g.* cholangiocarcinoma, metastases, etc), was also measured (16,17). The standard deviation of

the mean background signal on each image was corrected for the fact that images were constructed using a sum-of-squares method from an 8-channel phased-array coil (18). SNR in each tissue type was then calculated as a function of delay time and flip angle.

In order to identify the optimal delay time and flip angle for maximizing the contrast between the liver and either muscle or the bile ducts, the ratio of the SNRs between the tissue types ($SNR_{bile\ ducts}$ / SNR_{liver} and SNR_{liver} / SNR_{muscle}) was calculated and normalized to be 1 at the time of injection and at 15° flip angle. These particular ratios were chosen because $SNR_{bile\ ducts} > SNR_{liver} > SNR_{muscle}$. The delay time and flip angle that maximized $SNR_{bile\ ducts}$ / SNR_{liver} was considered optimal for visualizing the biliary system. Similarly, the parameters that maximized SNR_{liver} / SNR_{muscle} were considered optimal for visualizing non-hepatocyte origin neoplasms.

Evaluation of Clinical Implementation—The biliary-phase navigated 3D-SPGR images of the 51 studies ordered to assess known or suspected primary sclerosing cholangitis were scored by 2 radiologists with fellowship training in abdominal MRI with 6 and 9 years of experience in diagnostic imaging, using a consensus methodology. Overall image quality was scored on a 4-point Likert scale (0=non-diagnostic, 1=severe artifact [limiting diagnosis], 2=very mild artifact [not limiting diagnosis], 3=no significant artifact). Biliary excretion was also scored on a 4-point scale (0=none, 1=minimal gadolinium in bile ducts, 2=adequate for MR cholangiography, 3=excellent). Segmental non-excretion was noted (yes/no).

Since the flip angle and delay timing optimization was performed in healthy subjects, it is possible that image quality might be negatively affected in cases of severe biliary dysfunction. Because bilirubin is normally degraded and eliminated from the body through biliary excretion, elevated total serum bilirubin levels are often used clinically as a surrogate marker for biliary dysfunction. Therefore, each patient's medical record was reviewed for a total bilirubin measurement obtained within 90 days of the MRI. 28/51 (55%) of the patients had bilirubin levels drawn within this time frame, reflecting the local practice among our referring physicians. Image quality and biliary excretion scores in the patients having bilirubins below the median were compared with those in patients having bilirubins above the median.

Statistical Evaluation—Age and body weight of the subjects are reported as mean ± standard deviation over all subjects. For the flip angle optimization the normalized SNR ratios, summarized across all subjects, are reported as mean ± 95% confidence interval. Differences in the normalized SNR ratios were considered statistically significant if the mean ± 95% confidence intervals did not overlap. Plots of normalized SNR ratios versus delay time were also created in order to confirm previously reported results of the optimal time for imaging the biliary system using gadoxetic acid (14,15,19,20).

Artifact, biliary excretion, and preference scores are summarized as mean ± standard deviation. A paired two-tailed t-test was used to compare the artifact scores of the breath held with the navigated images. Two-tailed t-tests were used for the comparisons within the subset of clinical PSC cases that had bilirubin values measured within 90 days. A two-tailed t-test was used to compare the artifact scores obtained from the healthy subjects' navigated 3D-SPGR images with those obtained from the PSC patients' images. A p-value of <0.05 was considered statistically significant for each comparison.

RESULTS

Navigated 3D-SPGR

Figure 1 shows a representative example of a navigated 3D-SPGR acquisition, compared to both conventional (15° flip angle) and high flip angle (45°) breath-held 3D-SPGR acquisitions. The improved resolution of the navigated free-breathing acquisition (1.8mm vs 4mm slice thickness) is best appreciated on the coronal and sagittal reformations. Also, notice the subjectively higher SNR in the navigated 3D-SPGR images, acquired over ~5 min compared to the breath-held scans acquired over only 30 sec. The respiratory acceptance efficiency of the navigator acquisition in the healthy subject studies was 30–50%. The mean image quality score for the navigated 3D-SPGR acquisitions (2.26 ± 0.65) was slightly greater than the mean image quality score of the breath-held 3D-SPGR images (2.07 ± 0.65); however, this difference did not quite reach statistical significance (p=0.09) (Table 2). The raters preferred the navigated 3D-SPGR images in 29/46 (63%) of the paired comparisons and the breath-held images in 5/46 (11%), with 12/46 (26%) being scored as equivalent. The main differences between the two methods were the higher spatial resolution and subjectively higher signal in the optimized navigated 3D-SPGR images.

Optimal Delay Time

Figure 2a shows example images from a series of navigated 3D-SPGR acquisitions obtained from one of the healthy subjects over a 30-minute period after injection of gadoxetic acid. In 1/8 (12%) of the subjects, motion artifacts made it impossible to obtain time-course data and this case was excluded from the optimal delay time analysis. Figure 2b plots the SNR ratios in the 7/8 (88%) other subjects, normalized to the first measurement in each subject. The signal in the liver increases by a factor of 1.5 relative to muscle with a broad maximum occurring between 10–25 min following contrast injection. The signal in the bile ducts increases by a factor of 2.5–4.5 relative to liver with a broad maximum between 15–25 min following injection. These results are consistent with previously reported values (3,14,15,17,19–22).

Optimal Flip Angle

Figure 3a shows a series of images acquired at increasing flip angles for the same volunteer shown in Figure 2a. Figure 3b plots the mean normalized SNR ratios across all 8 subjects with 95% confidence intervals. Note that the normalized SNR of the bile ducts increases monotonically by a factor of 2 relative to liver as the flip angle increases from 15° to 45°. Similarly, the SNR in liver increases by a factor of 2 relative to muscle over the same flip angles. Statistically significant differences are present whenever the 95% confidence intervals do not overlap. As there was no statistically significant difference between the normalized SNR ratio at 40° and 45°, the decision was made to use 40° in the clinical implementation of the sequence in order to avoid possible SAR-related issues.

There were no appreciable differences in the measurements obtained with ascending flip angle order compared with descending flip angle order. The 25° repeat acquisitions following the other flip angle acquisitions were consistent with the earlier 25° measurements. These observations support the assumption that the observed SNR ratios were due entirely to differences in T1 weighting from differences in flip angle rather than to changes in tissue gadolinium concentration during the flip angle experiment. Images obtained with the higher flip angle are illustrated in the bottom two rows of Figure 1.

Clinical Implementation

Table 3 reports the image quality and biliary excretion scores recorded for all 51 clinical scans. Mean image quality score was 2.35 ± 0.82 (0=non-diagnostic, 1=severe artifact,

2=very mild artifact, 3=no significant artifact). This was not significantly different from the scores in the healthy subjects (p=0.54). Mean biliary excretion was 2.55 ± 0.97 (0=none, 1=minimal gadolinium in bile ducts, 2=adequate for MR cholangiography, 3=excellent). Segmental non-excretion of contrast into the bile was observed in 10/51 (20%) of the cases (*e.g.* Figure 4). Global non-excretion (biliary excretion score of 0 or 1) occurred in 7/51 (14%) patients.

Only 28/51 (55%) of patients had total bilirubin measured within 90 days of their MRI (13 ± 19 days, range: 0–67 days), due to clinical practice standards at our institution. 6/28 (21%) of these demonstrated segmental non-excretion, and 3/28 (11%) demonstrated global non-excretion – similar to the rates of decreased excretion seen amongst all 51 cases. Image quality and biliary excretion were not significantly affected by the total bilirubin level. Image quality in the 13/28 (46%) with total bilirubin < 0.7 was graded 2.46 ± 0.66 compared with 2.00 ± 0.93 in those with bilirubin ≥ 0.7 (p = 0.14). Biliary excretion was graded 2.92 ± 0.28 versus 2.33 ±1.23, respectively (p = 0.09). Of the 28 patients with serum bilirubin values drawn, the average bilirubin value was 1.40 ± 2.05 μmol/L (range = 0.30–10.80 μmol/L).

Figure 4 shows the case of a 35 year-old male with a known history of primary sclerosing cholangitis. This case illustrates the potential benefits of using the high-resolution free-breathing navigated 3D-SPGR sequence using optimized delay time and flip angle. In this case, a dominant stricture in a central branch of the right hepatic duct leads to segmental biliary obstruction with subsequent decreased hepatocyte function. These findings are easily visualized on delayed imaging as a wedge-shaped area of decreased signal within the liver parenchyma. The biliary system in this region does not enhance, suggesting that this is the most severe stricture and may be functionally significant. This additional information was highly complementary to the T2-weighted MRCP, which also demonstrated the stricture but provided no information on its functional significance. In addition, the extensive irregularity of the biliary ducts is clearly seen on thin-slab MIP images generated from the 20-min delayed navigated 3D-SPGR dataset. Of note, gadolinium contrast is visualized in the duodenum, also providing important functional information by demonstrating patency of the common duct. MIP images from the T2w 3D MRCP are provided for comparison. Note also the dual biliary and renal excretion of gadoxetic acid.

While none of the subjects specifically included in this study had cholangiocarcinoma, the potential benefits of using gadoxetic acid with a high resolution navigated 3D-SPGR pulse sequence with high flip angle and biliary phase imaging can be appreciated by analogy using another intrahepatic non-hepatocyte origin neoplasm. Figure 5 shows an example of a 51 year-old woman with known metastatic colorectal adenocarcinoma. As seen in this figure, metastases, similar to cholangiocarcinoma, contain no functioning hepatocytes and do not take up gadoxetic acid. They therefore appear as “dark holes” in a background of enhancing liver parenchyma on delayed T1-weighted imaging. This leads to a negative contrast, with very high conspicuity, particularly when compared to CT. Because vessels can also appear as “dark holes” on cross section in delayed gadoxetic acid enhanced images, minimum intensity projection (“minIP”) reconstructions of high spatial resolution navigated 3D-SPGR images are very helpful for identifying small lesions. The use of thin slab minIP reconstructions is analogous to the common use of thin slab MIP reconstructions for identification of pulmonary nodules on thoracic CT (23).

Finally, Figure 6 shows biliary phase pre-operative images of a 60 year-old male with a history of pancreatitis presumed to be due to cholelithiasis or choledocholithiasis. This example further illustrates the potential utility of the optimized navigated 3D-SPGR acquisition for characterizing biliary anatomy with high resolution T1w MR

cholangiograms. In this case, the optimized sequence enabled identification of two important biliary duct variants, either of which could have led to intra- or post-operative complications. Specifically, an anomalous posterior branch of the right intrahepatic bile duct joins the proper hepatic duct at the expected location of the cystic duct, while the cystic duct drapes across this anomalous duct and has a very low insertion into the common duct near the pancreatic head. In this particular case, the navigated 3D-SPGR acquisition provided better visualization of this biliary anomaly than the T2w MRCP performed during the same examination. The referring surgeon in this case stated that without this imaging result, he would have most likely have been misled by this variant anatomy into ligating the anomalous posterior branch of the right intrahepatic duct, believing it to be the cystic duct, causing biliary obstruction in the posterior right hepatic lobe and a potential bile leak from the non-ligated cystic duct. Note also that while 20-minute delayed images did not show filling of the gallbladder with contrast, after the patient was encouraged to walk for 10 minutes and reimaged at 45 minutes following contrast injection, the gallbladder had filled, demonstrating that there was no functional obstruction in the cystic duct, excluding the diagnosis of cholecystitis, analogous to the use of a nuclear medicine HIDA scan to exclude cholecystitis.

DISCUSSION

In this work, we have demonstrated the successful optimization and application of using a navigator-gated T1-weighted fat-saturated 3D-SPGR acquisition for very high spatial resolution imaging of the liver during the hepatobiliary phase after injection of gadoxetic acid contrast. Using this approach, we have obtained true spatial resolution of $1.2 \times 1.4 \times 1.8$ mm^3 (interpolated to $0.7 \times 0.7 \times 0.9$ mm^3) with excellent SNR and overall image quality, in approximately 5 minutes of free breathing. Asbach, *et. al.*, have previously described the use of a navigator for free-breathing liver imaging (15). However, that technique differed from the work described here by using a navigator-triggered inversion recovery prepared turbo-Flash sequence, a coronal navigator rather than a pencil beam navigator, a coronal acquisition slab, and a lower resolution ($1 \times 1 \times 1.5$ mm^3 interpolated – the true resolution before zero-filling was not specified). Further, Asbach, *et. al.*, did not perform optimization of the imaging flip angle to optimize SNR and CNR performance.

High spatial resolution images with near isotropic spatial resolution have the important advantage of being highly amenable to volume rendering methods and oblique multiplanar reformatting. In our experience, this capability has proven invaluable for visualization of hepatobiliary pathology, particularly small biliary structures and fine detail of focal hepatic lesions. Thin slab minIP images may also be helpful for visualization of small hepatic lesions because vessels, which appear round on thin slices, become elongated branching structures on minIP images, while focal lesions remain round, analogous to the use of MIPs for detection of pulmonary nodules on computed tomography (CT) (23).

A 0.05 mmol/kg dose of gadoxetic acid was used to maximize the enhancement performance on dynamic phase scans. Despite being twice the package insert dose, this is only half the dose of gadolinium routinely administered with a “single-dose” (0.1 mmol/kg) of gadobenate. Furthermore, based on our experience and the experience of others in the field (24–26), this dose is necessary for adequate tissue differentiation in the dynamic phase of hepatic imaging. In fact, a recent cross-over comparison study at 3T by Frydrychowicz, *et. al.* showed similar or slightly superior SNR and CNR performance with single-dose (0.1 mmol/kg) gadobenate compared with double-dose (0.05 mmol/kg) gadoxetic acid on dynamic phase liver imaging (17).

There are several limitations of our study. First, we have only performed the optimization for gadoxetic acid, whereas gadobenate also has significant hepatocyte uptake and biliary excretion. While the principles described above would also apply to hepatobiliary imaging with gadobenate, optimization of the timing and flip angle must also be performed. The dosing of gadobenate is typically higher (0.1 mmol/kg), while the fraction of contrast excreted in bile is lower (3–5%), and the relaxivity of the two agents are different (2,27). In addition, the timing of the peak hepatocyte and biliary phases is known to occur at approximately 1–2 hours (2), later than with gadoxetic acid. The large differences in dose and pharmacokinetics between gadoxetic acid and gadobenate require future optimization for gadobenate. The specific optimized values for imaging delay and flip angle described here for gadoxetic acid should not be applied to gadobenate.

Another limitation of this study is that rigorous examination of timing of contrast uptake in the hepatobiliary phase was only performed in volunteers with normal hepatic function. Gadoxetic acid uptake is thought to occur via the organic anionic transporting polypeptide 1 (OATP1) (28), which is known to compete with uptake of bilirubin into hepatocytes. For this reason, the timing and flip angle optimization performed in this study may not provide optimal image quality in patients with elevated bilirubin or hepatocyte dysfunction. For the same reason, however, decreased uptake and biliary excretion of contrast may provide important functional information on the liver (29), and we therefore advocate the use of uniform imaging protocols that have the potential to differentiate normal from abnormal liver. It was for this reason that we evaluated the image quality and biliary excretion seen using the optimized sequence in 51 consecutive scans performed to assess primary sclerosing cholangitis, a disease known to cause abnormalities in hepatobiliary function. The optimized sequence performed well in this setting, with no significant differences in image quality compared with the healthy volunteer scans. Furthermore, functional information regarding global and segmental biliary excretion was obtained and was complementary to the information provided by conventional T2w MRCP images (30). Regardless, further studies examining the uptake of hepatobiliary gadolinium agents in patients with liver disease and elevated bilirubin and their impact on optimized imaging protocols is warranted.

In the future, additional technical developments may prove helpful to further improve SNR, spatial resolution, and reduce scan time. The navigated sequence described in this work has been implemented with an autocalibrating parallel imaging reconstruction technique, known as autocalibrating reconstruction for Cartesian acquisition (ARC), that is capable of 2D acceleration using a full 3D kernel in *k*-space (31,32) with effective accelerations up to 3.75 easily achievable using an 8 channel coil (32). In this work, we chose not to use parallel imaging, both to maintain high SNR performance and also to facilitate valid SNR measurements, which are known to be difficult when parallel imaging methods are used (33). Future studies will examine the degree of acceleration than can be used while maintaining acceptable SNR and CNR.

In conclusion, we have demonstrated the technical feasibility of a navigator-based T1-weighted fat-saturated 3D spoiled gradient echo method for high spatial resolution imaging of the hepatobiliary phase of contrast-enhanced liver imaging using gadoxetic acid. Our approach may be a useful strategy to improve image quality and better exploit the behavior of new hepatobiliary contrast agents such as gadoxetic acid. Optimal hepatobiliary imaging occurs 15–25 minutes following contrast administration, with high flip angles in the 35–45° range providing significantly greater contrast of liver to either bile ducts or non-hepatocyte origin tumors.

Acknowledgments

Grant Support: NIH (R01 DK083380, R01 DK088925, RC1 EB010384), WARF Accelerator Program, Coulter Foundation

REFERENCES

1. Rofsky NM, Lee VS, Laub G, et al. Abdominal MR imaging with a volumetric interpolated breath-hold examination. Radiology. 1999; 212(3):876–884. [PubMed: 10478260]
2. Spinazzi A, Lorusso V, Pirovano G, Kirchin M. Safety, tolerance, biodistribution, and MR imaging enhancement of the liver with gadobenate dimeglumine: results of clinical pharmacologic and pilot imaging studies in nonpatient and patient volunteers. Acad Radiol. 1999; 6(5):282–291. [PubMed: 10228617]
3. Hamm B, Staks T, Muhler A, et al. Phase I clinical evaluation of Gd-EOB-DTPA as a hepatobiliary MR contrast agent: safety, pharmacokinetics, and MR imaging. Radiology. 1995; 195(3):785–792. [PubMed: 7754011]
4. Hammerstingl R, Huppertz A, Breuer J, et al. Diagnostic efficacy of gadoxetic acid (Primovist)-enhanced MRI and spiral CT for a therapeutic strategy: comparison with intraoperative and histopathologic findings in focal liver lesions. Eur Radiol. 2008; 18(3):457–467. [PubMed: 18058107]
5. Bluemke DA, Sahani D, Amendola M, et al. Efficacy and safety of MR imaging with liver-specific contrast agent: U. S. multicenter phase III study. Radiology. 2005; 237(1):89–98. [PubMed: 16126918]
6. Grazioli L, Morana G, Kirchin MA, Schneider G. Accurate differentiation of focal nodular hyperplasia from hepatic adenoma at gadobenate dimeglumine-enhanced MR imaging: prospective study. Radiology. 2005; 236(1):166–177. [PubMed: 15955857]
7. Zech CJ, Grazioli L, Breuer J, Reiser MF, Schoenberg SO. Diagnostic performance and description of morphological features of focal nodular hyperplasia in Gd-EOB-DTPA-enhanced liver magnetic resonance imaging: results of a multicenter trial. Invest Radiol. 2008; 43(7):504–511. [PubMed: 18580333]
8. Jung G, Breuer J, Poll LW, et al. Imaging characteristics of hepatocellular carcinoma using the hepatobiliary contrast agent Gd-EOB-DTPA. Acta Radiol. 2006; 47(1):15–23. [PubMed: 16498928]
9. Kim JI, Lee JM, Choi JY, et al. The value of gadobenate dimeglumine-enhanced delayed phase MR imaging for characterization of hepatocellular nodules in the cirrhotic liver. Invest Radiol. 2008; 43(3):202–210. [PubMed: 18301317]
10. Akpinar E, Turkbey B, Karcaaltincaba M, et al. Initial experience on utility of gadobenate dimeglumine (Gd-BOPTA) enhanced T1-weighted MR cholangiography in diagnosis of acute cholecystitis. J Magn Reson Imaging. 2009; 30(3):578–585. [PubMed: 19711404]
11. Gupta RT, Brady CM, Lotz J, Boll DT, Merkle EM. Dynamic MR imaging of the biliary system using hepatocyte-specific contrast agents. AJR Am J Roentgenol. 2010; 195(2):405–413. [PubMed: 20651197]
12. Frydrychowicz A, Lubner MG, Brown JJ, et al. Hepatobiliary MR imaging with gadolinium-based contrast agents. J Magn Reson Imaging. 2012; 35(3):492–511. [PubMed: 22334493]
13. McKenzie CA, Lim D, Ransil BJ, et al. Shortening MR image acquisition time for volumetric interpolated breath-hold examination with a recently developed parallel imaging reconstruction technique: clinical feasibility. Radiology. 2004; 230(2):589–594. [PubMed: 14699184]
14. Dahlstrom N, Persson A, Albiin N, Smedby O, Brismar TB. Contrast-enhanced magnetic resonance cholangiography with Gd-BOPTA and Gd-EOB-DTPA in healthy subjects. Acta Radiol. 2007; 48(4):362–368. [PubMed: 17453513]
15. Asbach P, Warmuth C, Stemmer A, et al. High spatial resolution T1-weighted MR imaging of liver and biliary tract during uptake phase of a hepatocyte-specific contrast medium. Invest Radiol. 2008; 43(11):809–815. [PubMed: 18923261]
16. Runge VM. A comparison of two MR hepatobiliary gadolinium chelates: Gd-BOPTA and Gd-EOB-DTPA. J Comput Assist Tomogr. 1998; 22(4):643–650. [PubMed: 9676461]

17. Frydrychowicz A, Nagle SK, D'Souza SL, Vigen KK, Reeder SB. Optimized high-resolution contrast-enhanced hepatobiliary imaging at 3 tesla: A cross-over comparison of gadobenate dimeglumine and gadoxetic acid. J Magn Reson Imaging. 2011; 34(3):585–594. [PubMed: 21751288]
18. Dietrich O, Raya JG, Reeder SB, Ingrisch M, Reiser MF, Schoenberg SO. Influence of multichannel combination, parallel imaging and other reconstruction techniques on MRI noise characteristics. Magn Reson Imaging. 2008; 26(6):754–762. [PubMed: 18440746]
19. Reimer P, Rummeny EJ, Shamsi K, et al. Phase II clinical evaluation of Gd-EOB-DTPA: dose, safety aspects, and pulse sequence. Radiology. 1996; 199(1):177–183. [PubMed: 8633143]
20. Nagle, SK.; Busse, RF.; Brau, AC., et al. High-resolution free-breathing 3D T1 weighted hepatobiliary imaging optimized for Gd-EOB-DTPA. Proceedings of the 18th Annual Meeting of ISMRM; Honolulu. 2009. (abstract 2076)
21. Carlos RC, Branam JD, Dong Q, Hussain HK, Francis IR. Biliary imaging with Gd-EOB-DTPA: is a 20-minute delay sufficient? Acad Radiol. 2002; 9(11):1322–1325. [PubMed: 12449364]
22. Carlos RC, Hussain HK, Song JH, Francis IR. Gadolinium-ethoxybenzyldiethylenetriamine pentaacetic acid as an intrabiliary contrast agent: preliminary assessment. AJR Am J Roentgenol. 2002; 179(1):87–92. [PubMed: 12076911]
23. Kawel N, Seifert B, Luetolf M, Boehm T. Effect of slab thickness on the CT detection of pulmonary nodules: use of sliding thin-slab maximum intensity projection and volume rendering. AJR Am J Roentgenol. 2009; 192(5):1324–1329. [PubMed: 19380557]
24. Lee MS, Lee JY, Kim SH, et al. Gadoxetic acid disodium-enhanced magnetic resonance imaging for biliary and vascular evaluations in preoperative living liver donors: comparison with gadobenate dimeglumine-enhanced MRI. J Magn Reson Imaging. 2011; 33(1):149–159. [PubMed: 21182133]
25. Brismar TB, Dahlstrom N, Edsborg N, Persson A, Smedby O, Albiin N. Liver vessel enhancement by Gd-BOPTA and Gd-EOB-DTPA: a comparison in healthy volunteers. Acta Radiol. 2009; 50(7):709–715. [PubMed: 19701821]
26. Motosugi U, Ichikawa T, Sano K, et al. Double-dose gadoxetic Acid-enhanced magnetic resonance imaging in patients with chronic liver disease. Invest Radiol. 2011; 46(2):141–145. [PubMed: 21139506]
27. Rohrer M, Bauer H, Mintorovitch J, Requardt M, Weinmann HJ. Comparison of magnetic properties of MRI contrast media solutions at different magnetic field strengths. Invest Radiol. 2005; 40(11):715–724. [PubMed: 16230904]
28. van Montfoort JE, Stieger B, Meijer DK, Weinmann HJ, Meier PJ, Fattinger KE. Hepatic uptake of the magnetic resonance imaging contrast agent gadoxetate by the organic anion transporting polypeptide Oatp1. J Pharmacol Exp Ther. 1999; 290(1):153–157. [PubMed: 10381771]
29. Takao H, Akai H, Tajima T, et al. MR imaging of the biliary tract with Gd-EOB-DTPA: Effect of liver function on signal intensity. Eur J Radiol. 2011; 77(2):325–329. [PubMed: 19726150]
30. Jedynak, AR.; Kelcz, F.; Frydrychowicz, A.; Nagle, SK.; Reeder, SB. Clinical experience with gadoxetate-enhanced T1 weighted hepatobiliary imaging in primary sclerosing cholangitis. Proceedings of the 19th Annual Meeting of ISMRM; Stockholm, Sweden. 2010. (abstract 2620)
31. Brau AC, Beatty PJ, Skare S, Bammer R. Comparison of reconstruction accuracy and efficiency among autocalibrating data-driven parallel imaging methods. Magn Reson Med. 2008; 59(2):382–395. [PubMed: 18228603]
32. Lum DP, Busse RF, Francois CJ, et al. Increased volume of coverage for abdominal contrast-enhanced MR angiography with two-dimensional autocalibrating parallel imaging: initial experience at 3.0 Tesla. J Magn Reson Imaging. 2009; 30(5):1093–1100. [PubMed: 19856443]
33. Reeder SB, Wintersperger BJ, Dietrich O, et al. Practical approaches to the evaluation of signal-to-noise ratio performance with parallel imaging: application with cardiac imaging and a 32-channel cardiac coil. Magn Reson Med. 2005; 54(3):748–754. [PubMed: 16088885]

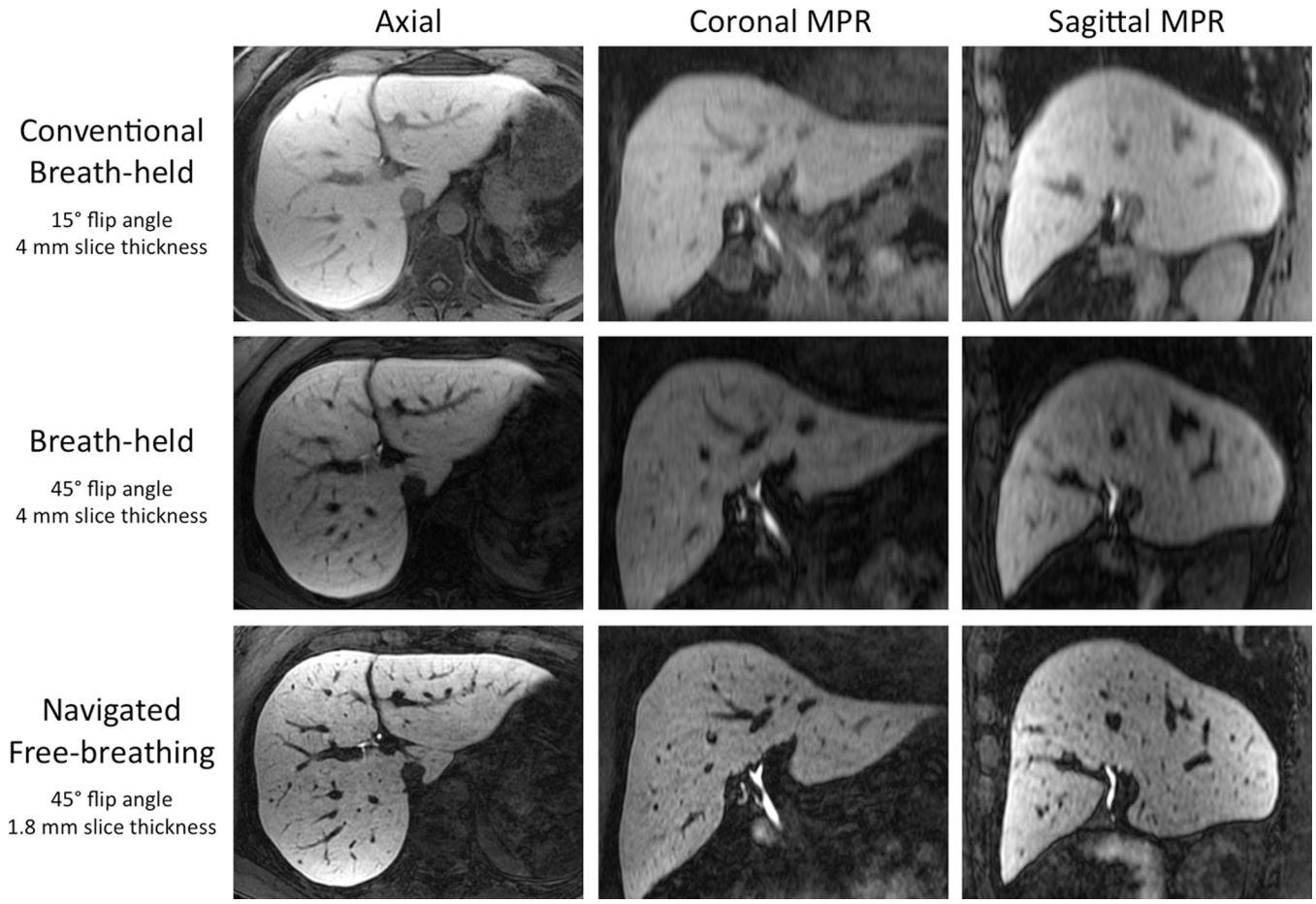

Figure 1. Multiplanar reformations

Multiplanar reformations of conventional flip angle breath-held (top row), flip angle optimized breath-held (middle row), and flip angle optimized free-breathing navigated sequences (bottom row) demonstrate both 1) improved contrast using a higher flip angle and 2) improved spatial resolution and subjective SNR using the navigated free-breathing 3D-SPGR sequence acquired over ~5 min. Separate window/level settings were used for each row of images. Note the absence of any saturation effects due to the navigator pulse.

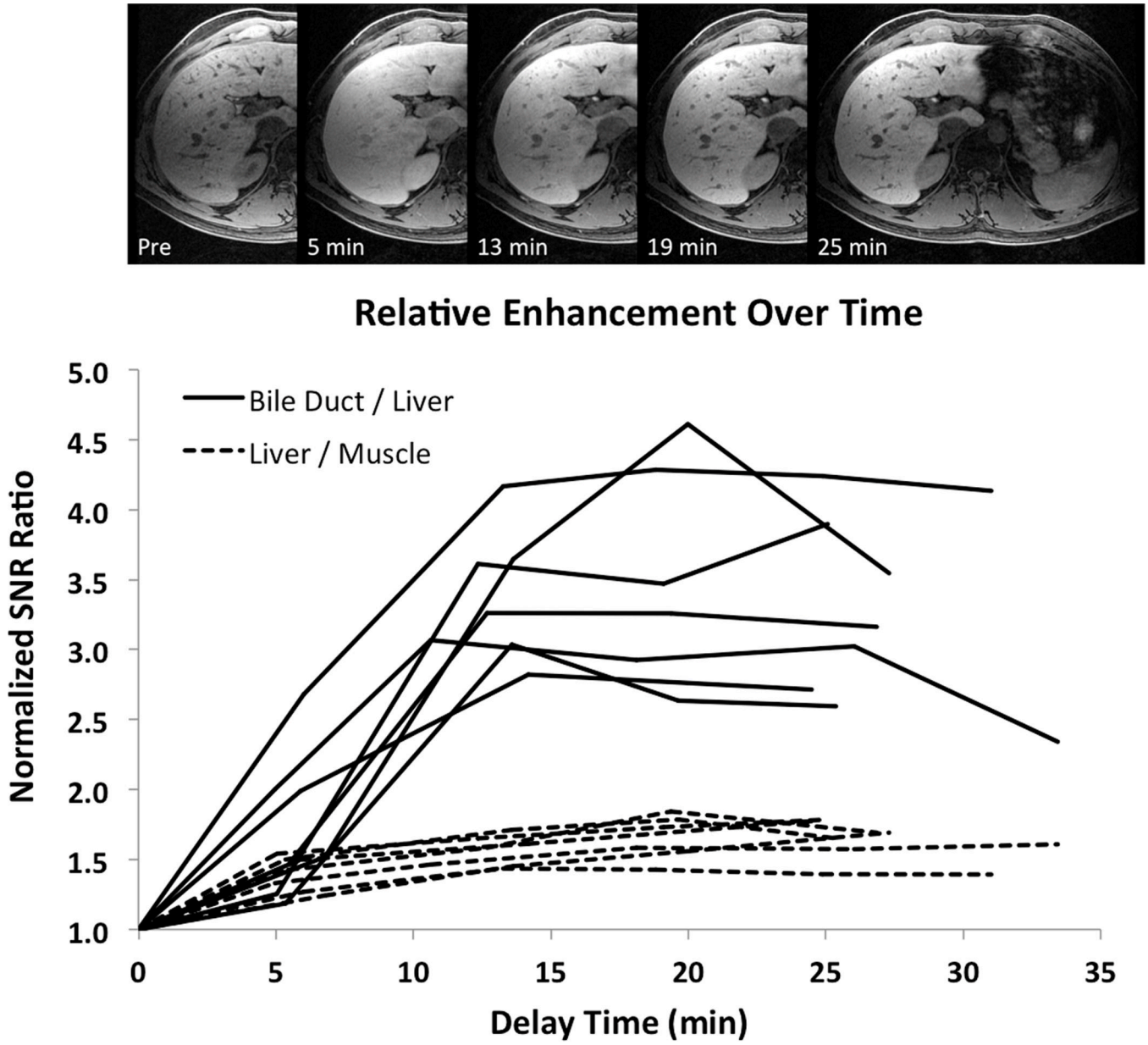

Figure 2. Delay Time Optimization

Images show the uptake of gadoxetic acid over time in one of the 8 healthy subjects, obtained using the 3D high-resolution T1-weighted navigated 3D-SPGR sequence. The plot shows the relative SNR ratios of bile ducts and muscle compared with liver for all 7/8 (88%) of the technically adequate studies. While the liver signal increases by a factor of 1.5 compared with muscle over 10–25 min following injection, the signal in the bile ducts increases by a factor of 2.5–4.5, peaking between 15–25 min.

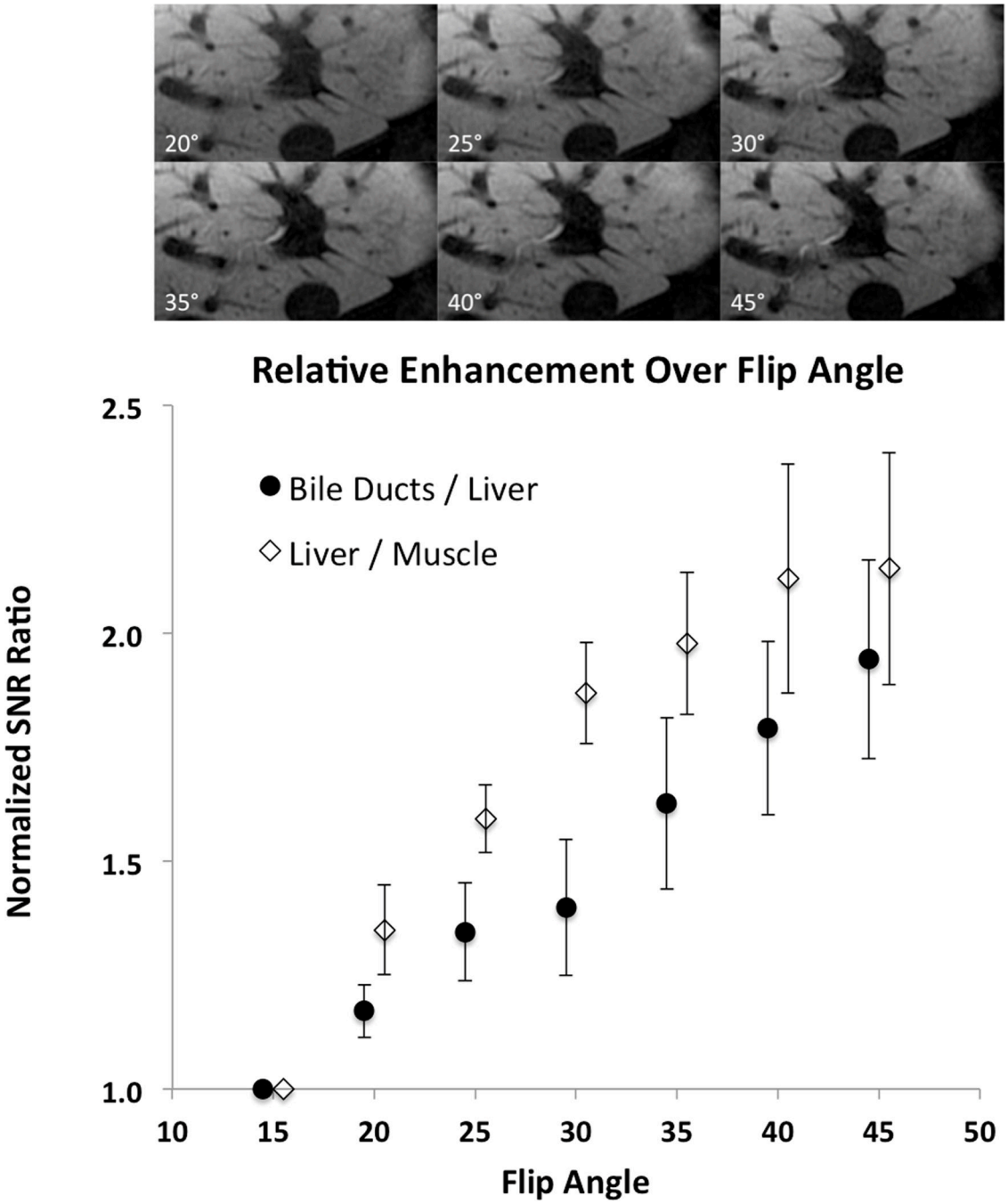

Figure 3. Flip Angle Optimization

Images obtained by varying the flip angle in the same healthy subject as shown in Figure 2. The plot of SNR ratios shows statistically significant monotonic increases as a function of flip angle. This results in increased contrast between liver and both bile ducts and non-hepatocyte origin intrahepatic tumors such as cholangiocarcinoma. Because the increase in the SNR ratios between 40° and 45° degrees was not statistically significant, a 40° flip angle was chosen for the optimized clinical protocol in order to avoid any potential SAR issues.

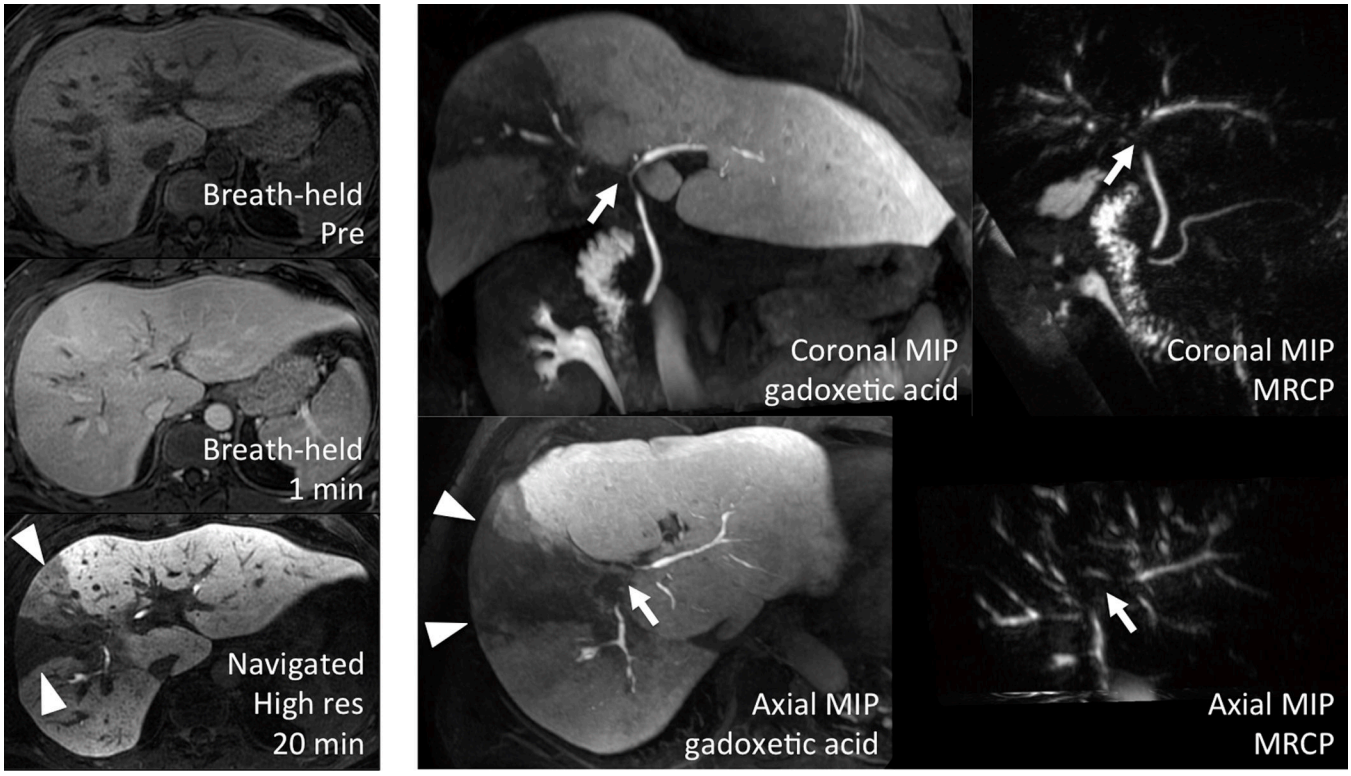

Figure 4. Primary sclerosing cholangitis

Functional information regarding both hepatocyte function and biliary patency can be gained from the use of gadoxetic acid and the optimized navigated 3D-SPGR acquisition. Note the wedge (triangles) of non-excretion corresponding to the dominant stricture (arrows) on MRCP. Note also gadolinium present in the duodenum, indicating that bile is able to reach the bowel.

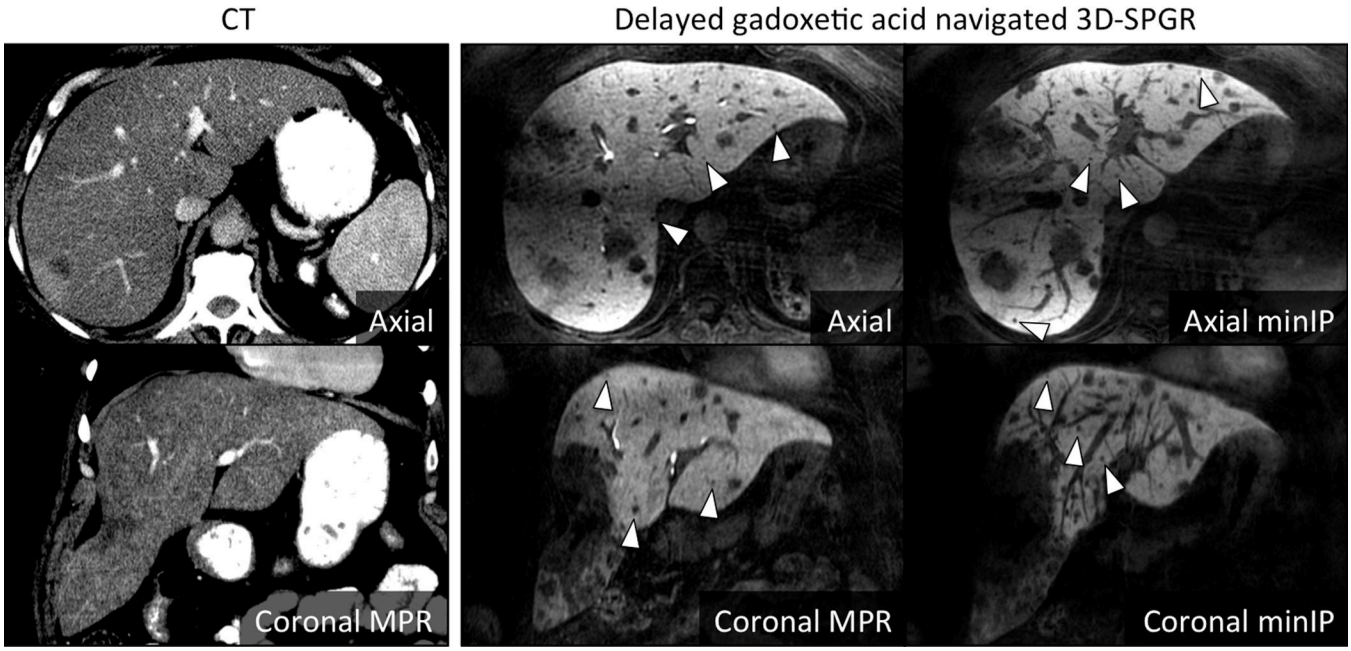

Figure 5. Visualization of non-hepatocyte origin intrahepatic neoplasm

In this patient with colorectal adenocarcinoma metastases, the high conspicuity of the low signal lesions against the high signal liver is apparent. Note the small size of the lesions (arrowheads) made more apparent on the minimum intensity projection images (right panels), many of which were undetectable on CT (left panels).

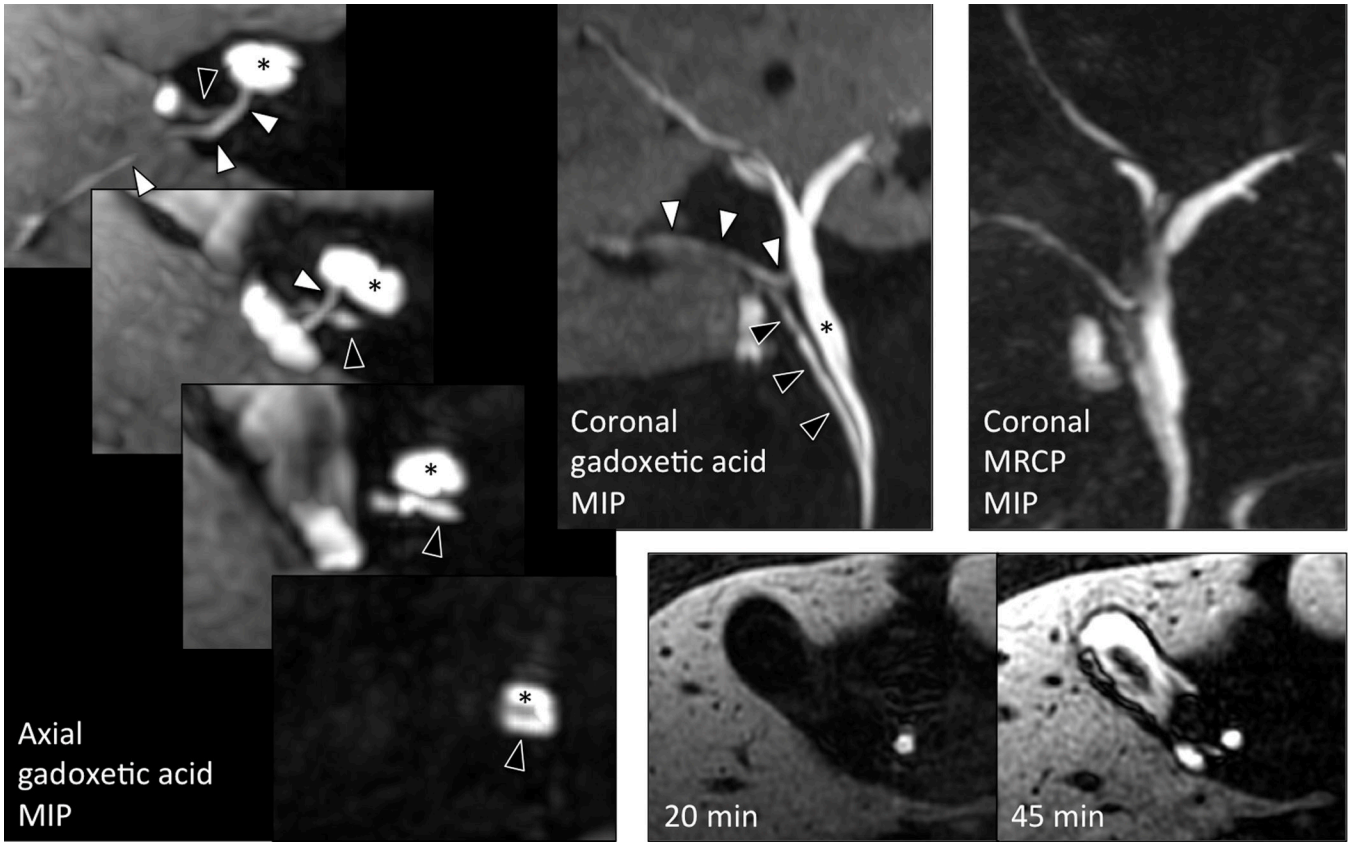

Figure 6. Visualization of biliary anatomy

In this patient with suspected gallstone pancreatitis, the posterior right intrahepatic bile duct (white arrowhead) drains anomalously into the common hepatic duct (*) at the expected location of the cystic duct. The cystic duct itself (black arrowhead) demonstrates a very low insertion to the common hepatic duct in the pancreatic head. This anatomy was more easily appreciated on the navigated 3D-SPGR acquisition than on T2-weighted MRCP. Contrast filled the gallbladder on 45-min delayed imaging, demonstrating that there was no functional obstruction in the cystic duct and therefore no evidence of cholecystitis.

Table 1

Scan Parameters

Acquisitions were performed at 1.5T clinical scanner (Signa HDx, v14.0, GE Healthcare, Waukesha, WI) using an 8-channel cardiac coil. No parallel imaging was used.

	Breath-held 3D-SPGR	Navigator-gated 3D-SPGR
TR	5.5 ms	
TE	2.6 ms	
Matrix (RL × AP × SI)	288 × 224 × 44	288 × 256 × 104
FOV (RL × AP × SI)	35 × 28 × 18 cm^3	
BW	±42 kHz	
Partial Fourier	0.70	0.75
True Resolution	1.2 × 1.6 × 4.0 mm^3	1.2 × 1.4 × 1.8 mm^3
Interpolated Resolution	0.7 × 0.7 × 2.0 mm^3	0.7 × 0.7 × 0.9 mm^3
Scan Time	30 sec	5–6 min

Table 2

Healthy Subjects

Image quality scores for the navigated and breath-held 3D-SPGR acquisitions. 46 paired comparisons were possible because navigated and breath-held acquisitions were alternated in all 8 subjects for approximately 30 minutes following injection in order to determine optimal timing for hepatobiliary phase imaging. While the mean image quality score for the navigated acquisition was higher than for the breath-held acquisition, this difference did not quite reach statistically significant (p=0.09).

	Image Quality					
	0	**1**	**2**	**3**	**Mean Score**	**Preferred**
Navigator-gated	0	5	24	17	2.26 ± 0.65	63%
Breath-held	0	8	27	11	2.07 ± 0.65	11%

0 = non-diagnostic
1 = severe artifact
2 = very mild artifact
3 = no significant artifact

Table 3

Primary Sclerosing Cholangitis Patients

Image quality and biliary excretion scores for the clinical studies. Image quality scores in these 51 cases did not differ from the image quality scores in the healthy subjects (p=0.54). The image quality and biliary excretion scores were not significantly affected by the total bilirubin level (p=0.14 and p=0.09, respectively).

		Image Quality					Biliary Excretion					Segmental non-excretion
	N	0	1	2	3	Mean	0	1	2	3	Mean	
All Patients	51	0	11	11	29	2.35 ± 0.82	5	2	4	40	2.55 ± 0.97	10 (20%)
Patients with Serum bilirubin	28	0	7	8	13	2.21 ± 0.83	3	0	2	23	2.61 ± 0.96	6 (21%)
Bilirubin < 0.7	13	0	1	5	7	2.46 ± 0.66	0	0	1	12	2.92 ± 0.28	2 (15%)
Bilirubin ≥ 0.7	15	0	6	3	6	2.00 ± 0.93	3	0	1	11	2.33 ± 1.23	4 (27%)

0 = non-diagnostic
1 = severe artifacts
2 = very mild artifacts
3 = no significant artifacts

0 = none
1 = minimal
2 = adequate for MRC
3 = excellent